Supplement of Earth Syst. Sci. Data, 12, 2517–2536, 2020
https://doi.org/10.5194/essd-12-2517-2020-supplement

Open Access Earth System Science Data

Supplement of

Apparent ecosystem carbon turnover time: uncertainties and robust features

Naixin Fan et al.

Correspondence to: Naixin Fan (nfan@bgc-jena.mpg.de) and Nuno Carvalhais (ncarval@bgc-jena.mpg.de)

Supplementary material

S1 Mass conservative aggregation

In order to correctly unify the spatial resolutions and geographic coordinate systems of the datasets from different sources we used a mass conservative aggregation method. In this approach, the total amount/mass of a stock (i.e. soil and vegetation) does not change during spatial aggregation and transformation of the data. Note that this approach is only followed for data that are expressed in mass per unit area of a grid cell. First, a variable (X), in units of mass per unit area, to be aggregated from the original fine resolution (X_{fine}) is multiplied by a corresponding grid cell area at the same resolution (A_{fine}), as shown in equation (1). Then the product at the fine resolution (XA_{fine}) is aggregated by summing all the finer grid cells within a larger target coarse grid (equation (2)). This aggregated product will be in N⨯N matrix size which depends on the target resolution. Similarly, the area of the target grid cell is calculated by summing the areas of all the fine grid cells within it (equation (3)). Finally, the area-weighted mean for the variable at the target resolution is calculated by dividing aggregated coarse product (XA_{coarse}) with a corresponding land area (A_{coarse}), as shown in equation (4).

$$XA_{fine} = X_{fine} \times A_{fine} \quad (1)$$

$$XA_{coarse} = SUM(XA_{fine}) \quad (2)$$

$$A_{coarse} = SUM(A_{fine}) \quad (3)$$

$$XA_{coarse} = \frac{XA_{coarse}}{A_{coarse}} \quad (4)$$

The method was applied to all soil and vegetation carbon and GPP datasets (see Section 2 of the manuscript) that required aggregation.

S2 Bulk density correction

The bulk density (BD) estimates in SoilGrids and LandGIS are too high due to two reasons. First, there are relatively fewer measurements of BD, missing in several horizons (Hengl et al., 2017). In addition, there are known problems with measurements of BD in permafrost regions of Canadian and Eurasian high latitudes, especially in forest regions with high organic carbon (Tomislav Hengl, pers. comm.). In this study, we applied a pedotransfer function from Köchy et al. (2015) to make correction based on organic carbon concentration:

$$BD = \left(1.38 - 0.31 \times \log\left(\frac{OC}{10}\right)\right) \times 1000 \quad (5)$$

where, OC is the soil organic carbon content in percentage. Note that the correction was only applied in the grid cells with OC > 8%.

S3 Model selection for extrapolation of soil

In this section, we introduce the framework used to select the models for extrapolating soil carbon from 0 – 2 m depth to the full soil depth.

S3.1 Different characteristics of permafrost and non-permafrost soil

In general, the amount and vertical distribution of soil organic carbon are largely influenced by the vegetation which fixes atmospheric CO_2 and transfers carbon into the land ecosystems. However, the storage of soil organic carbon (SOC) has a more complex relationship with primary productivity (Jackson et al., 2017). The higher biomass, which implies more carbon sequestration by aboveground biomass, however, does not necessarily lead to increases in SOC storage, as would be under assumption of linear increase. Although the processes of soil formation, accumulation, and stabilization have been extensively studied and debated, modeling and parameterizing the simulation of mechanisms that determine the geographical and vertical distribution of SOC, especially in deeper soil, is still unclear at global scales. Therefore, instead of using process-based models, we employed statistical approaches and empirical mathematical models to estimate SOC at full depth from the globally available 2 m estimates. Such approach is needed since the available datasets of soil carbon only cover until a maximum of 2 m depth and the amount of carbon stored in deeper soil, which may have feedback to climate in the decadal to longer timescales, depending on the local SOC stabilization mechanisms, is still unknown. The other reason is that different datasets report SOC stock until different depths, and a direct comparison requires the harmonization of representative soil depths.

To characterize the vertical distribution of SOC, we used 425 permafrost peatland profiles from ISCN soil database (Nave et al., 2017) and 1000 profiles from WOSIS soil database (Batjes et al., 2019). Figure S1 shows the accumulated SOC stock profiles with depth in permafrost and non-permafrost regions. The vertical distribution of carbon with depth in the permafrost region shows a distinct feature of a linear relationship between SOC and soil depth that is not apparent in non-permafrost profiles. This behavior translates strong stabilization mechanisms, likely the long-term result of temperature and hydrological controls on decomposition processes and implies that the SOC may continue to be large beyond the depth of 3 m in the permafrost regions (Figure S1b). However, due to limited observations in permafrost peatlands, it is unclear to what depth the SOC concentrations are significant and to which extent a limited depth consideration affects the estimates of total SOC in these regions. In contrast, most of the soil profiles in the non-permafrost region stop increasing before the depth of 2 m (Figure S1c).

S3.2. Estimating global SOC at full depth

We included 12 different empirical mathematical models (Table S1) to predict total SOC storage to the full soil depth. All the models were used to fit all the soil profiles in WOSIS and ISCN databases (see Figure S1 for observed data, and Figure S2 for an example of model fitting for a soil profile). Despite the significant fit in each model there is a potential large range of model predictions at full depth (Figure S2). We, therefore, tested two different model averaging methods to obtain the best representative SOC ensemble prediction until the full soil depth:

1. The equal weights averaging (EWA) method, in which all models are given equal weights and the ensemble prediction is simply calculated as the average of all model predictions, tests the fitness of all possible model combinations to achieve the best model ensemble for predicting SOC at full depth.
2. The Bayesian model averaging (BMA) method (Vrugt, 2016), which explicitly considers the uncertainty of prediction of a target variable and provides a probabilistic distribution of weights for each model instead of a single deterministic weight as in the EWA method. By maximizing the likelihood function from the training dataset, the weights $\beta = \{\beta 1, \ldots, \beta k\}$ and standard deviation $\sigma = \{\sigma 1, \ldots, \sigma k\}$ are estimated. In the BMA approach, models with non-significant contributions to the ensemble fit are discarded. We used the BMA method included in the MODELAVG Matlab toolbox (Vrugt, 2016).

The best model ensembles are obtained using the criteria to maximize MEF, minimize KL, and minimize AIC. The results show that EWA and BMA methods have similar performances (Table S2). Given the similarities in the statistical performance between methods, but the larger fraction of observations within prediction uncertainty (larger Coverage in Table S2) here we select the EWA method.

We conducted two different batches of experiments to consider the differences between the circumpolar and non-circumpolar datasets (see above section S3.1): (i) fitting the models using the observational data points down to 50 cm depth to estimate the SOC at full soil depth (beyond 100 cm) for non-circumpolar regions (Figure S3); and (ii) fitting the models using the observational data points down to 200 cm depth to predict the SOC at full soil depth (beyond 200 cm) for circumpolar regions (Figure S4). This is an approach that can be reproduced at every grid-cell and is here applied to the in-situ data to assess the overall robustness of SOC estimates at full depth.

Two model ensembles were selected after using the EWA method to best represent the SOC vertical distribution, one for the circumpolar and non-circumpolar regions; results synthesized in Figures S3 and S4, respectively. Figure S3 shows the robustness of the ensemble including DIJKL to predict the SOC at full depth in the non-circumpolar region using the data points up to 50 cm depth. The modelling efficiency was 0.90 and with a small normalized root mean square error (NRMSE). The histogram (Figure S3b) of SOC distribution at full depth shows a similar distribution between the predictions and observations, with a small positive bias (Figure S3c), which is revealed in the statistical difference between predictions and observations (Figure S3b). Overall, more than 60% of observations were found to be within the uncertainty range of the prediction ensemble. The results show that the best ensemble represents the vertical distribution of C_{soil} in most sites. For the circumpolar region the best ensemble included ACDEF models. The results show that the overall model performance of the

best ensemble in the circumpolar region is weaker in comparison to the non-circumpolar ensemble. In these regions, the modelling efficiency was 0.64 with a small NRMSE (Figure S4a). The histogram (Figure S4b) of SOC distribution at full depth shows qualitatively similar but statistically different distributions of predictions and observations, with a positive bias (Figures S4b and c). These results show a reduction in performance when compared to the model ensemble for the non-circumpolar regions, while still explaining 77% of the spatial variability at site scales across soil profiles.

Based on these results, the models selected for each of the ensembles (DIJKL for the non-circumpolar and ACDEF for circumpolar regions) were then fitted to the vertical distribution of SOC per grid cell in each grid cell to predict the full depth SOC for each of the three global SOC datasets: Sanderman, SoilGrids and LandGIS.

References

Jackson, R. B., Lajtha, K., Crow, S. E., Hugelius, G., Kramer, M. G., and Piñeiro, G.: The ecology of soil carbon: pools, vulnerabilities, and biotic and abiotic controls, Annual Review of Ecology, Evolution, and Systematics, 48, 419-445, 2017.

Hengl, T., de Jesus, J. M., Heuvelink, G. B., Gonzalez, M. R., Kilibarda, M., Blagotić, A., Shangguan, W., Wright, M. N., Geng, X., and Bauer-Marschallinger, B.: SoilGrids250m: Global gridded soil information based on machine learning, PloS one, 12, e0169748, 2017.

Köchy, M., Hiederer, R., and Freibauer, A.: Global distribution of soil organic carbon–Part 1: Masses and frequency distributions of SOC stocks for the tropics, permafrost regions, wetlands, and the world, Soil, 1, 351-365, 2015.

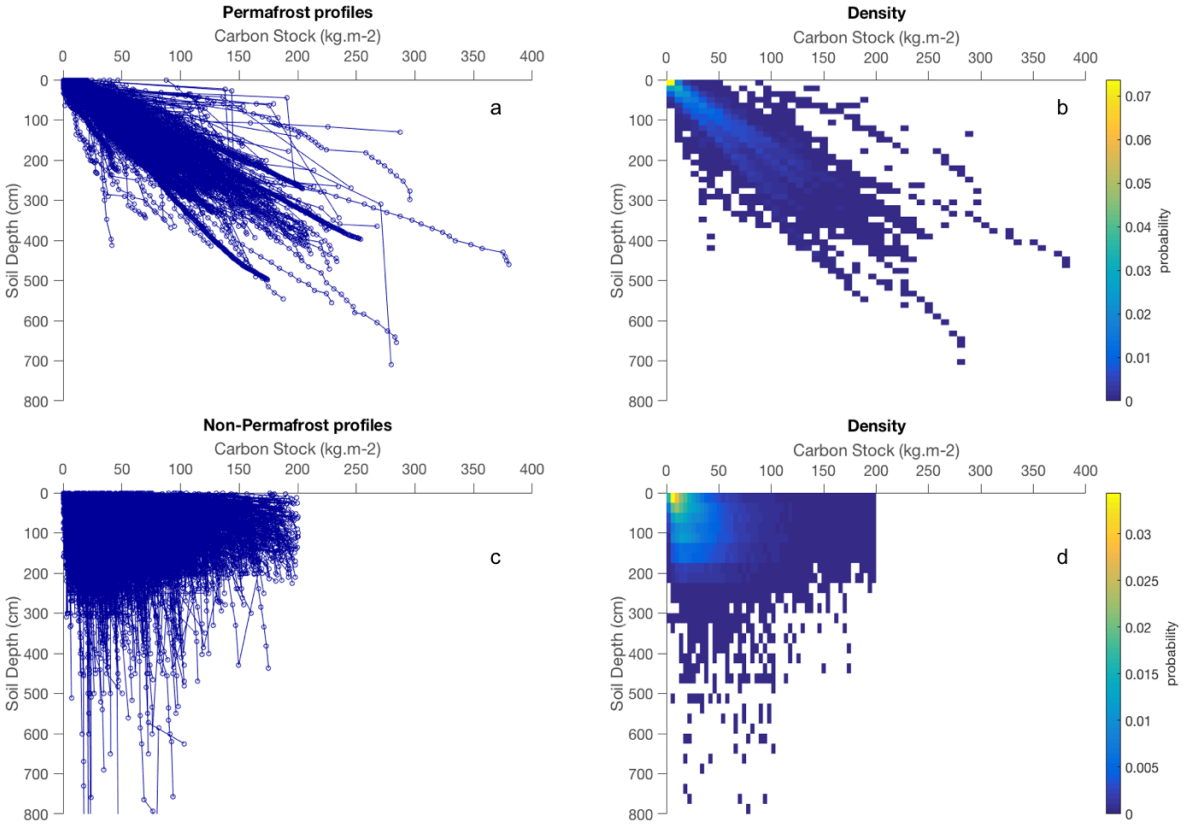

Figure S1: The observed vertical distribution of accumulated SOC stock (kg.m-2) with depth (cm). (a) 425 soil profiles of the permafrost peatland region from ISCN database and (c) 1000 soil profiles of the non-permafrost region from WOSIS database. The corresponding distribution densities of SOC are presented in b and d. The blue open circle in the profiles represents observational data points.

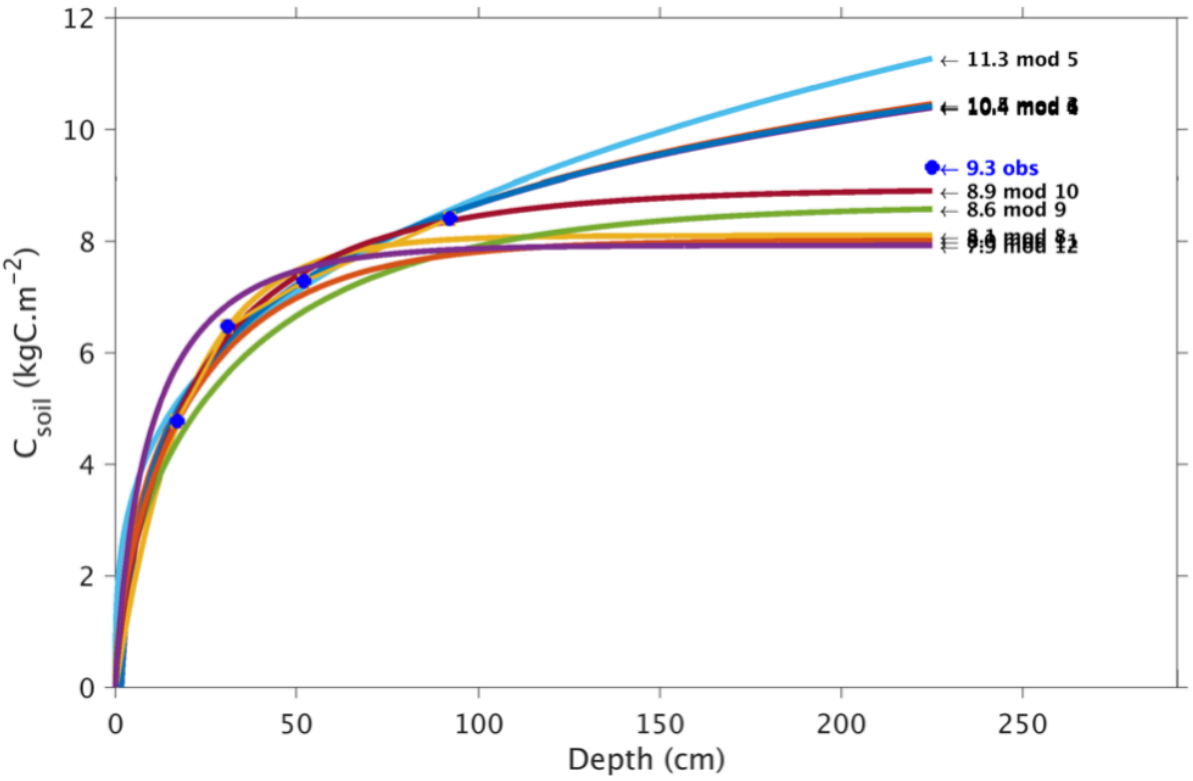

Figure S1: An example of observed and modelled soil profiles. The colored lines are different models, and the blue dots are the observation points.

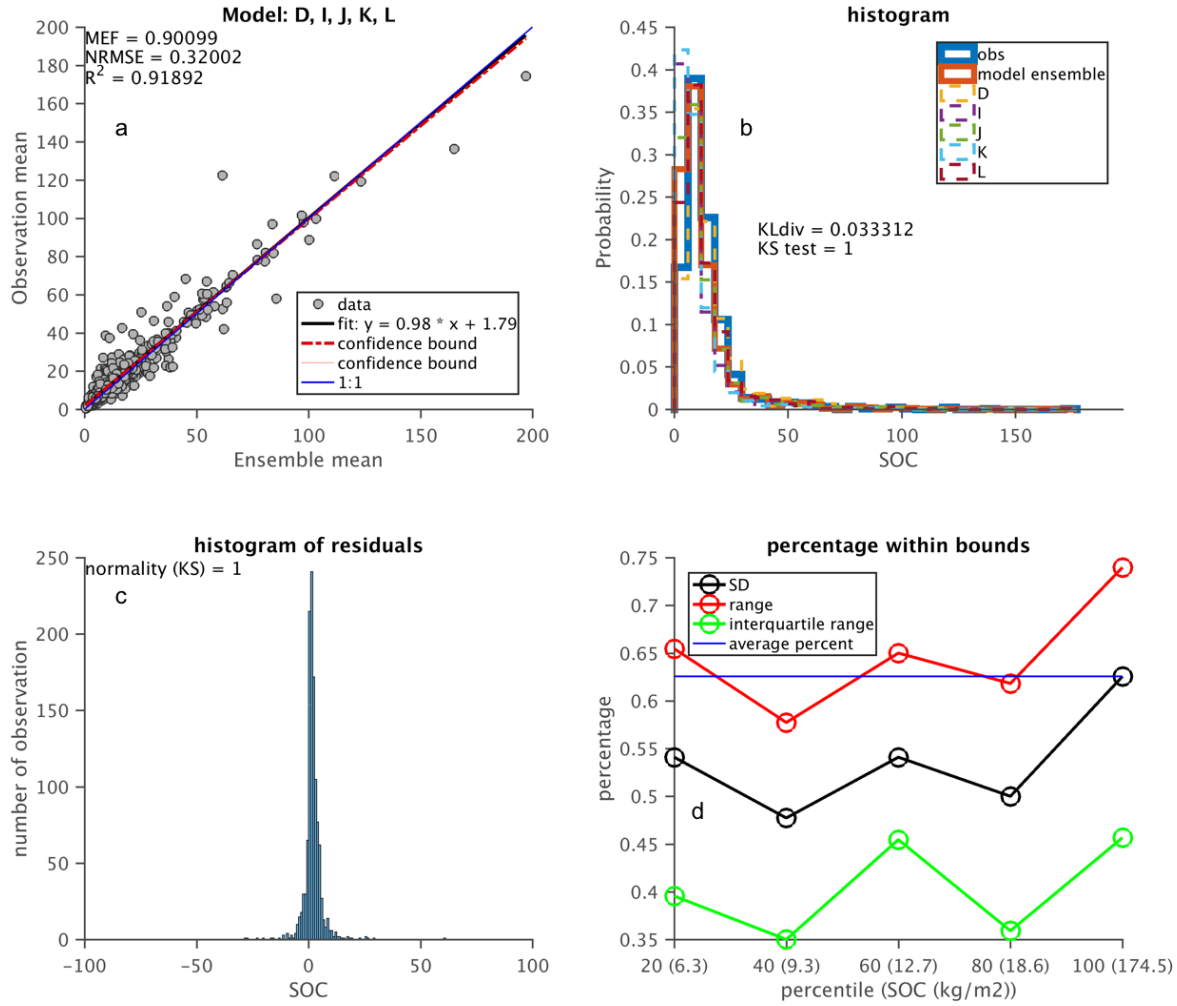

Figure S3: Performance of the averaged results of model D, I, J, K and L in predicting soil carbon storage to full depth using WOSIS data in the non-circumpolar region. (a) Ensemble mean vs. observation, 1:1 line in blue. (b) The histogram of observation, model ensemble and each model. It shows the Kullback-Leibler distance from model ensemble mean to observation, the two-sample Kolmogorov-Smirnov test (a value of 0 means that one cannot reject the hypothesis that the output from the model ensemble and the observations come from the same distribution; 1 means otherwise). (c) residue between model ensemble mean and observation. (d) The coverage of observation data points within [-σ, +σ], [min, max], [25%, 75%] and average.

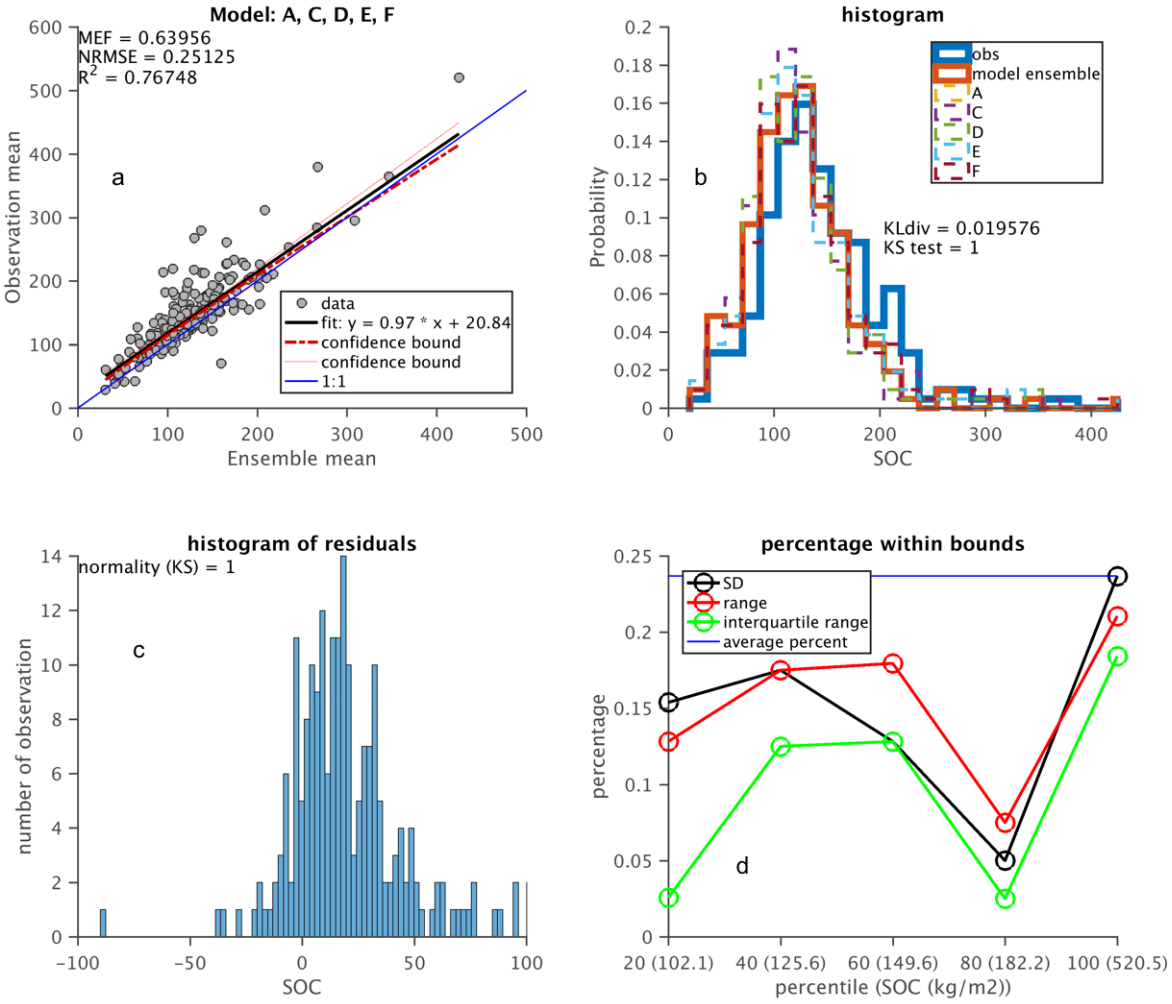

Figure S4: The same as Figure S3 except for using ISCN data in the circumpolar region. Note that model ensemble includes the predictions of A, C, D, E and F models to predict soil carbon storage from 200cm to deep soil.

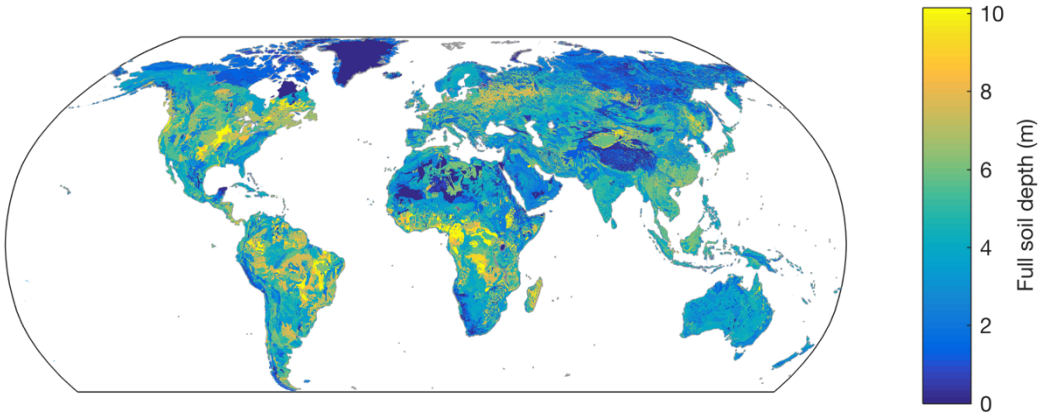

Figure S5: Global distribution of full soil depth from Webb (2000).

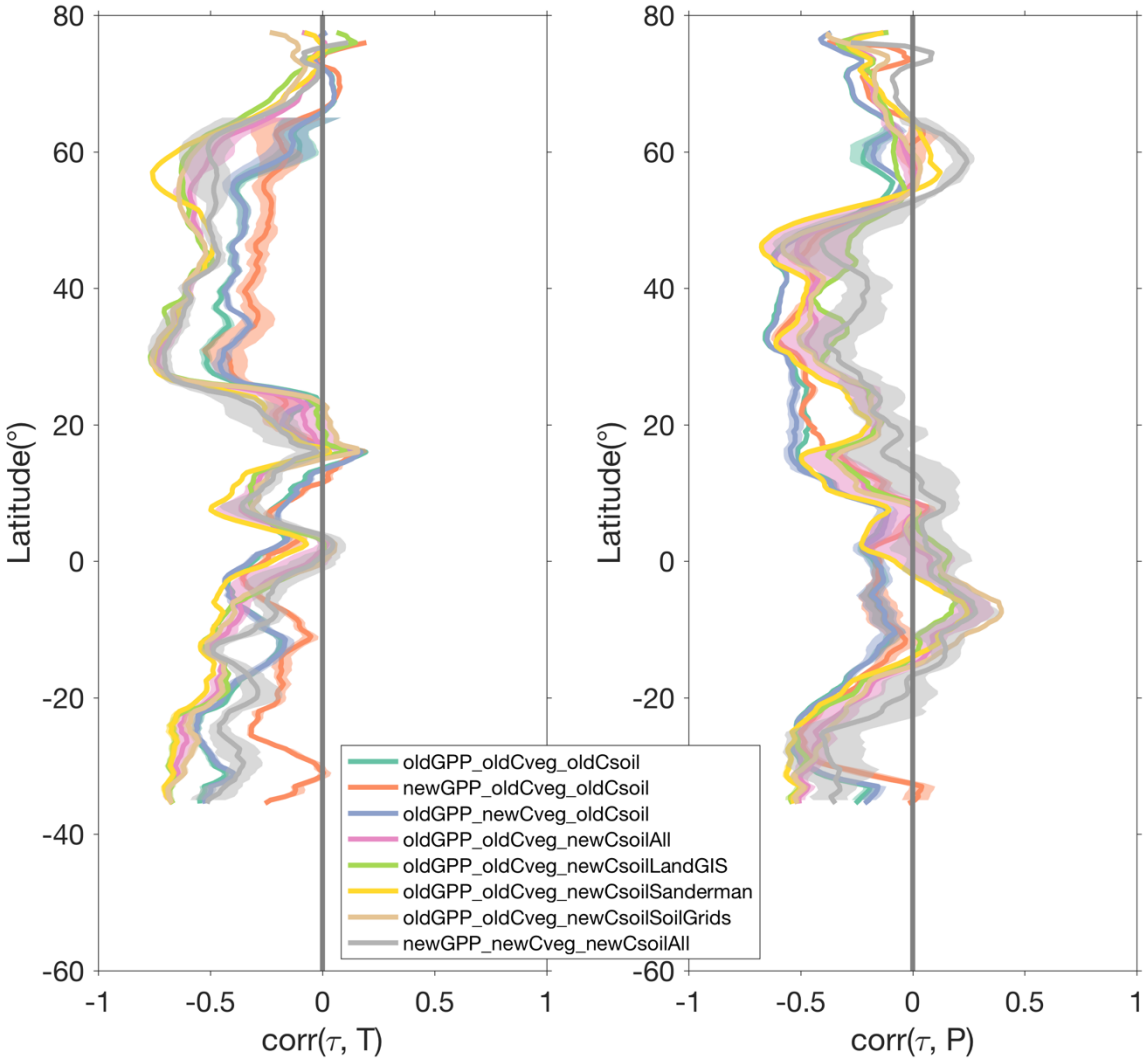

Figure S6: Comparison of the zonal correlation between τ and climate with the previous study (Carvalhais et al., 2014)**.** Each component (C_{soil}, C_{veg} and GPP) from the previous study is mixed with each component of the current study. The prefix 'old' stands for the component from the previous study and the prefix 'new' stands for the component from the current study.

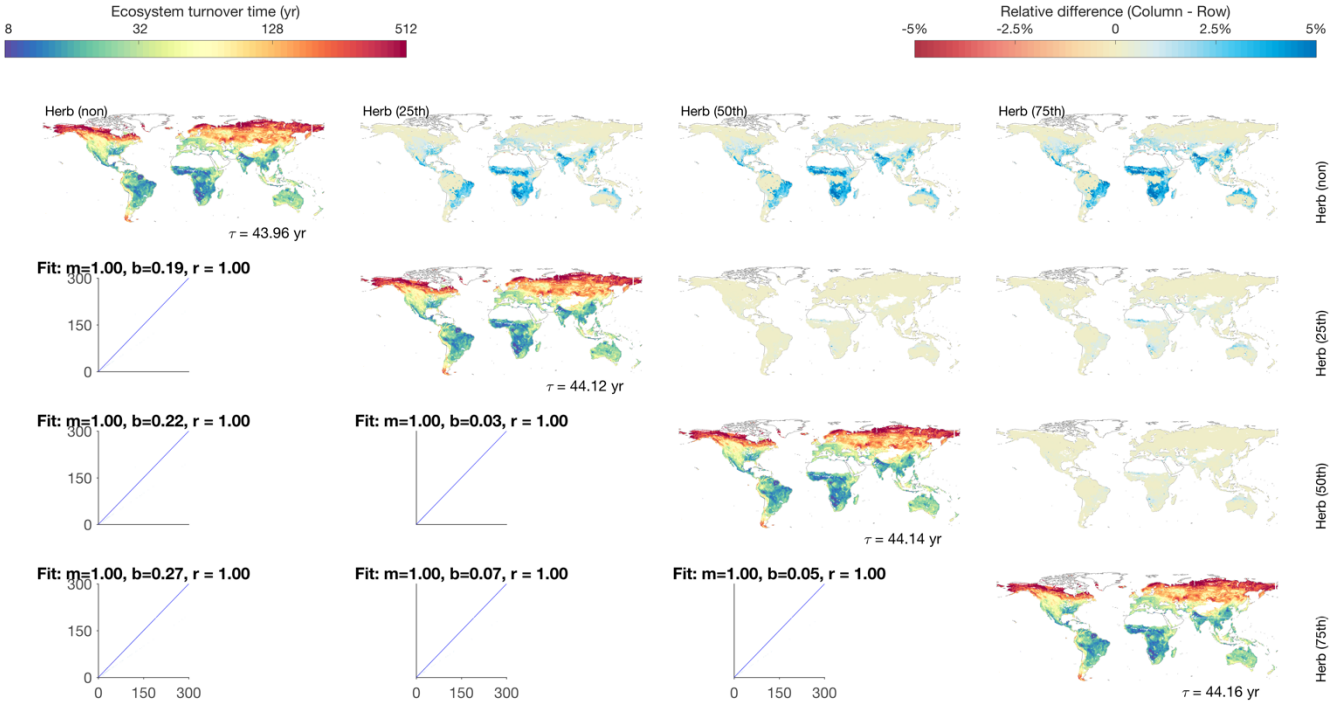

Figure S7: The spatial distribution of turnover times with different estimates of herbaceous carbon stocks. The turnover times are estimated with no herbaceous component ("Herb (non)"), herbaceous components based on the different percentiles of GPP estimates: 25th ("Herb (25th)"), 50th ("Herb (50th)"), 75th ("Herb (75th)"). The global turnover times are shown in the bottom of each diagonal subplot. The upper off-diagonal subplots are the ratios between each pair of datasets (column/row). The bottom off-diagonal subplots show the major axis regression between each pair of datasets (m: slope, b: intercept, r: Pearson correlation coefficient). The ranges of both of the colorbars approximately span between the 1st and the 99th percentiles of the data. Hereafter, all figures comparing different spatial maps include the information in a similar manner.

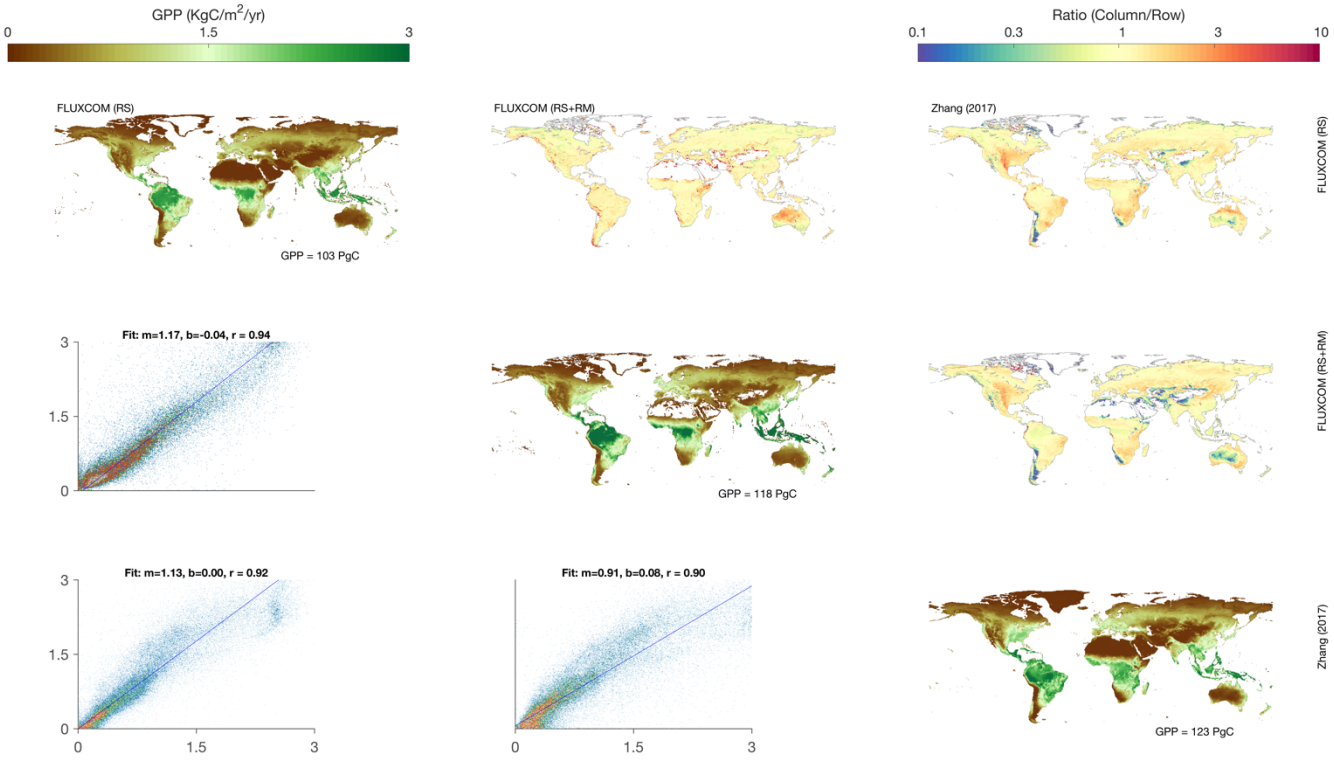

Figure S8: Comparison of the mean annual GPP estimates from FLUXCOM and Zhang et al., 2017. Refer to caption of Figure S7 for details on the information plotted in the figure.

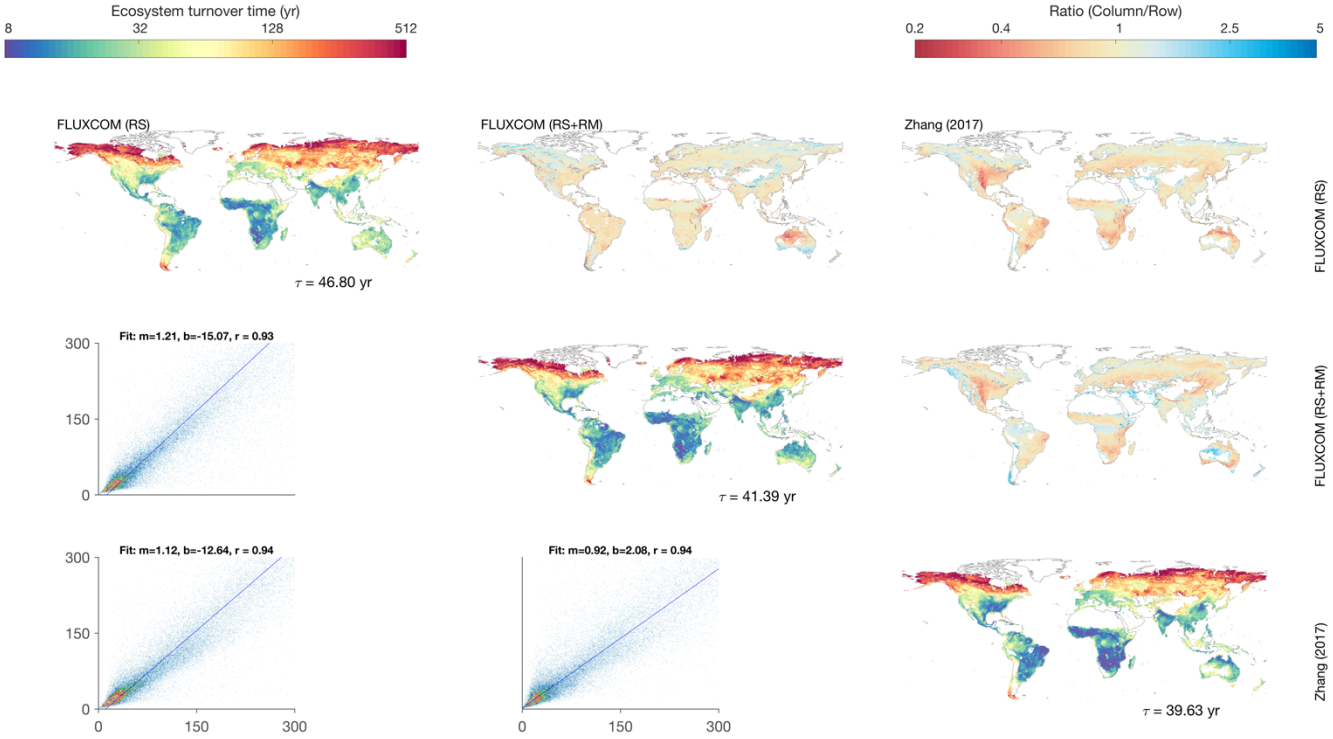

Figure S9: Comparison of the spatial distribution of turnover times using different GPP products. The GPP products are compared in Figure S8.

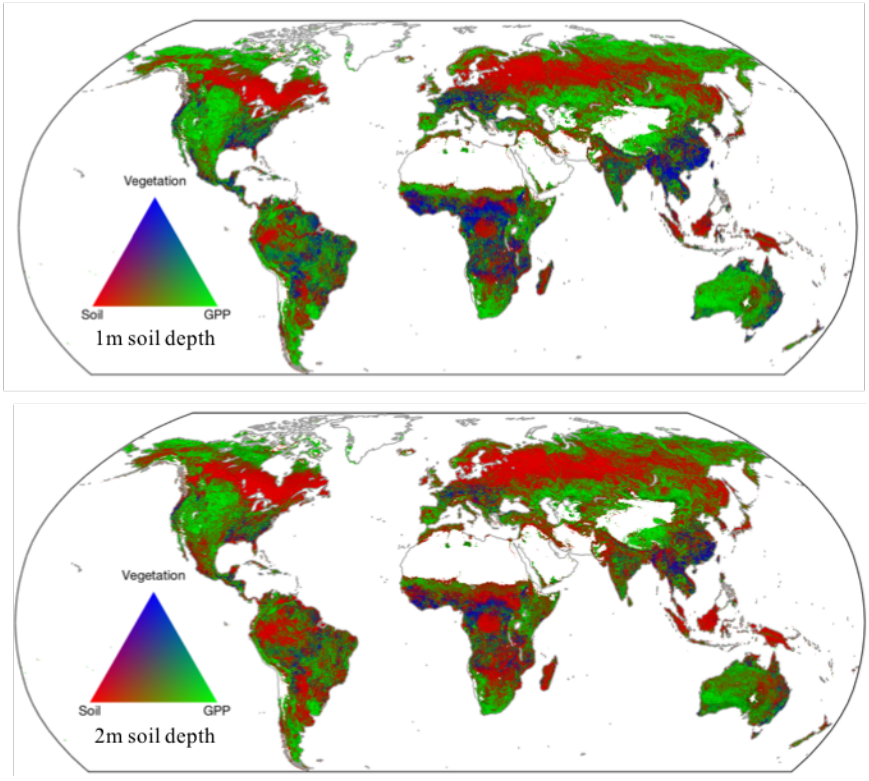

Figure S10: Local sources of uncertainties in τ estimates for different soil depth assumptions: (top) 1m and (bottom) 2m. The contribution of each source of uncertainty (soil, vegetation and GPP) is determined as in Methods Section 3.4. The green color indicates the regions where the uncertainty is dominated by GPP, red by soil carbon, and blue by vegetation carbon.

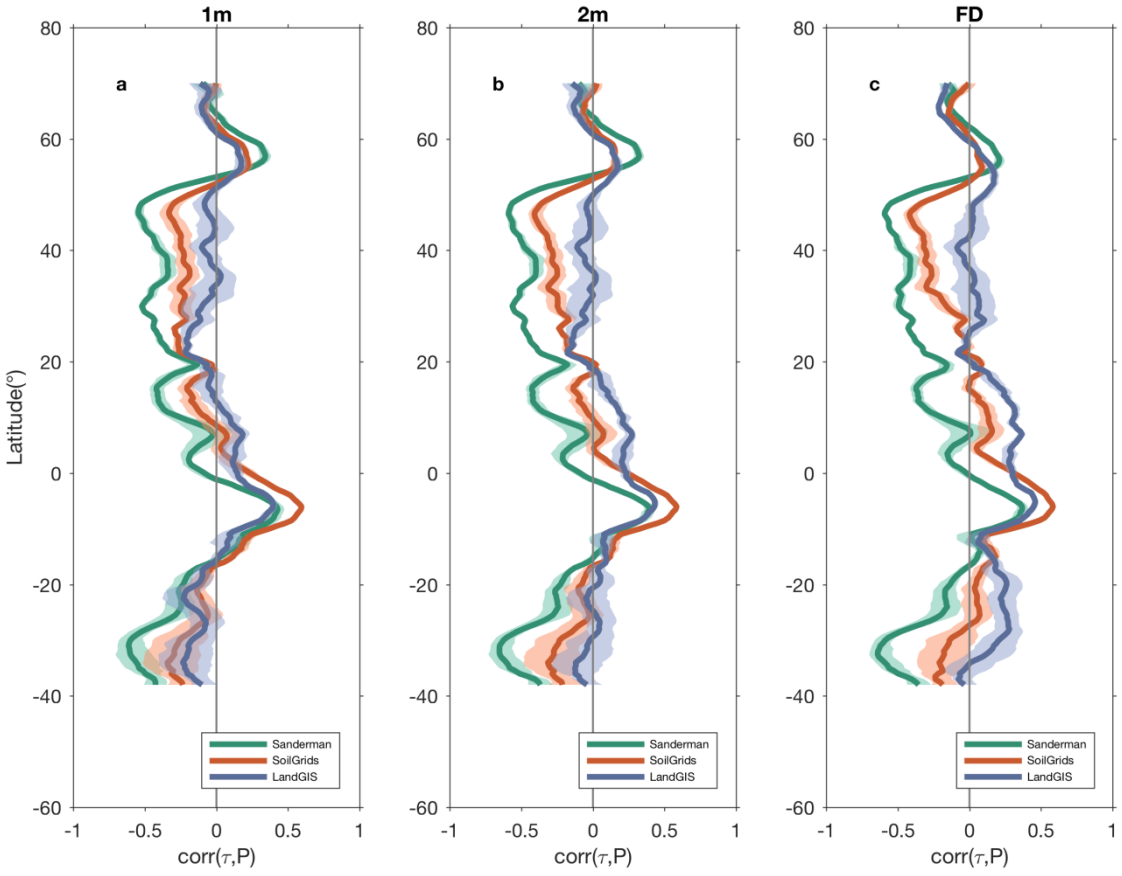

Figure S11: The zonal correlation between τ and mean annual precipitation (P) using different soil depths and sources of soil carbon data. For details on the data, see Section 2 of the main text.

Table S1: Empirical mathematical models used for extrapolation of soil carbon to full soil depth.

Model identifier	Equation
A	$a \cdot D^b + C$
B	$a \cdot e^{b \cdot D} + c \cdot e^{d \cdot D}$
C	$a \cdot log(b \cdot D + 1)$
D	$a \cdot log(b \cdot D + c)$
E	$K \cdot log_{10}(D) + I$
F	$(10^I \cdot D^{K+1})/(K+1) + c$

G	$a + b \cdot D$
H	$b \cdot (1 - \beta^D)$
I	$b \cdot (1 - \beta^D)^a$
J	$a \cdot (1 - e^{-(D/b)^c})$
K	$a \cdot (1 - e^{-b \cdot D})^c$
L	$a \cdot (1 - \frac{log\ log\ (1 - (1 - b) \cdot e^{-c \cdot D})}{log(b)})$

Table S2: Performance of different model ensembles in the circumpolar and non-circumpolar regions.

	Circumpolar		Non-circumpolar	
	EWA	**BMA**	**EWA**	**BMA**
RMSE	36.575	37.686	5.482	5.292
AIC	1516.134	1528.526	3977.226	3895.513
KL	0.020	0.020	0.039	0.036
MEF	0.640	0.617	0.862	0.872
Coverage (%)	14.5	13.5	61.9	50.3

Table S3: Contributions of different components to the total uncertainties in turnover times (in %) at the global and regional scales. The results are also summarized when different soil depths (1 m, 2 m, and full soil depth) are considered.

	1m			**2m**			**FD**		
	Circumpolar	Non-circumpolar	Global	Circumpolar	Non-circumpolar	Global	Circumpolar	Non-circumpolar	Global
C_{soil}	67.69	41.96	72.28	68.98	62.37	79.57	72.11	79.51	84.20
C_{veg}	0.07	1.90	0.38	0.02	0.58	0.11	0.02	0.21	0.06
GPP	31.13	55.95	27.08	29.87	36.77	20.01	26.69	19.93	15.43